Upper-State-Assisted Uphill Energy Transfer in a Far-Red Light-Harvesting Antenna from an Antarctic Alga

Yusuke Yoneda[1,2], Makiko Kosugi[2,3], Jun Minagawa[2,3], Hikaru Kuramochi[1,2,4]*

[1]Research Center of Integrative Molecular Systems (CIMoS), Institute for Molecular Science, National Institutes of Natural Sciences, 38 Nishigo-Naka, Myodaiji, Okazaki 444-8585, Japan.

[2]Graduate Institute for Advanced Studies, SOKENDAI, 38 Nishigo-Naka, Myodaiji, Okazaki 444-8585, Japan.

[3]Division of Environmental Photobiology, National Institute for Basic Biology, 38 Nishigo-Naka, Myodaiji, Okazaki 444-8585, Japan.

[4]Graduate School of Engineering Science, The University of Osaka, 1-3 Machikaneyama-cho, Toyonaka 560-8531, Japan

*yyoneda@ims.ac.jp

ABSTRACT

Photosynthetic organisms thrive across remarkably diverse light environments, from dim, spectrally filtered habitats to high-irradiance niches. Their antenna complexes have evolved structural and excitonic features that tailor energy capture and delivery to local conditions, making comparative studies of noncanonical antennas essential for understanding the diversity of evolved designs. Here we investigate the far-red light-harvesting complex from an Antarctic alga *Prasiola crispa* (Pc-frLHC), whose ring-shaped undecameric (11-subunit) antenna absorbs strongly near ~710 nm yet still drives Photosystem II. Using femtosecond transient absorption with selective excitation of chlorophyll (Chl) *b* (645 nm), Chl *a* (675 nm), and far-red Chls (740 nm), we resolve a rapid, directional energy transfer cascade that funnels population into the lowest excitonic level of the far-red Chl trimer. Transient absorption anisotropy directly resolves a characteristic hopping time between the far-red Chl trimers of ~11.5 ps, while exciton–exciton annihilation kinetics under increased fluence at far-red excitation provide independent corroboration. Spectral dynamics and anisotropy further reveal the existence of a higher-lying excitonic state near ~670 nm within the far-red Chls. Thermal access to this ~670 nm state enables repeated cycling that facilitates the uphill transfer toward Chl *a* despite a sizable energy gap of ~580 cm^{-1}. These findings clarify how Pc-frLHC exploits the excitonic coupling and the ring-mediated transport to harvest red-shifted light to Photosystem II, offering general principles for engineering photofunctional systems adapted to spectrally limited environments.

I. INTRODUCTION

Photosynthetic organisms have evolved a wide array of light-harvesting antenna complexes (LHCs) to thrive in diverse and often extreme environments.[1–3] Across photosynthetic organisms, antenna systems adjust to local light fields through pigment composition, excitonic coupling, and protein architecture, yielding diverse solutions for capturing and routing excitation. In eukaryotes, photosystem I (PSI) is commonly served by the light-harvesting chlorophyll protein complexes of PSI (LHCI) that can host long-wavelength forms of chlorophyll (Chl) extending absorption toward ~720 nm,[4–6] whereas photosystem II (PSII) typically draws on excitations near ~680 nm and its associated LHCII generally lacks such long-wavelength forms. As a result, effective PSII excitation by far-red photons (~700–800 nm) has been considered uncommon, though notable algal cases have been documented.[7–9] These contrasting strategies underscore the tunability of antenna design and highlight the importance of elucidating how photosynthetic systems harvest and direct low-energy photons to PSII, identifying what combinations of pigment choices, excitonic interactions, and protein scaffolds enable uphill delivery with sufficient rate and yield.

Prasiola crispa (*P. crispa*), one of the major green algae in Antarctica,[10,11] showcases a particularly striking adaptation: its unique antenna complex, Pc-frLHC, exhibits strong absorption in the far-red region (~710 nm), significantly red-shifted compared to the primary absorption peak of PSII reaction centers found in most green plants and algae (FIG. 1).[12] This red-shifted absorption enables *P. crispa* to efficiently capture the residual light that reaches the interior of its densely packed colonies, microenvironments where visible wavelengths are scarce but where the organism is shielded from environmental extremes such as intense radiation, freezing temperatures, and desiccation. Remarkably, despite harvesting such low-energy photons, Pc-frLHC still drives oxygenic photosynthesis via PSII,[13] a capability that is crucial for sustaining photosynthetic function in *P. crispa* under polar conditions. This raises intriguing questions

about how excitation energy is funneled uphill, from far-red-absorbing pigments to the PSII reaction center.

Recent cryo-electron microscopy (cryo-EM) analysis of the Pc-frLHC at 3.13 Å resolution has unveiled a highly distinctive supramolecular architecture.[12] The antenna forms an undecameric (11-mer) ring of eleven Pc-frLHC monomers, each with four transmembrane helices and coordinating eleven Chls, predominantly Chl *a* with a minor complement of Chl *b*, and two carotenoids (FIG. 1a, b). This structural organization markedly differs from the typical trimeric LHCII and instead bears evolutionary similarity to LHCI-type antennas found in *Chlamydomonas reinhardtii*, particularly the four-helix Lhca2 subunit.[14] A defining feature of Pc-frLHC is its far-red absorption centered around 710 nm, which has been attributed to a strongly coupled Chl trimer (603, 609, and 708). A recent computational study suggests that this trimer forms an excitonically coupled unit exhibiting substantial charge-transfer character, leading to a significant redshift of the Q_y transition.[15] Complementary time-resolved fluorescence spectroscopy previously suggested the possibility of uphill energy transfer from these far-red absorbing Chls to higher-energy Chl *a* states.[12] This counterintuitive process has been proposed to be driven by entropy-assisted mechanisms, in which thermal fluctuations and state degeneracy enable energy transfer against the intrinsic energy gradient, supporting directional energy flow toward the PSII. However, because fluorescence-based methods are limited in temporal resolution and are insensitive to excitonic states with weak radiative signatures, the microscopic details of uphill transfer, particularly the roles of fast excitonic dynamics and pigment–pigment coupling, have remained elusive.

In this study, we investigated the excited-state dynamics of Pc-frLHC using femtosecond transient absorption spectroscopy. By selectively exciting Chl *b* (645 nm), Chl *a* (675 nm), and far-red Chls (740 nm), we tracked the sequence and timescale of energy transfer among pigments. Furthermore, the possibility of uphill energy transfer was assessed by examining exciton–exciton annihilation dynamics

and transient absorption anisotropy. These complementary approaches revealed the presence of a higher-lying excitonic state near 670 nm arising from the far-red Chls, which appears to mediate rapid energy exchange and facilitate thermally assisted uphill transfer toward Chl *a*, ultimately guiding excitation energy toward PSII under low-energy light conditions. This study highlights an antenna strategy for light utilization in spectrally limited environments and provides mechanistic insight into how red-shifted antennas contribute to photosynthetic efficiency through excitonic interaction.

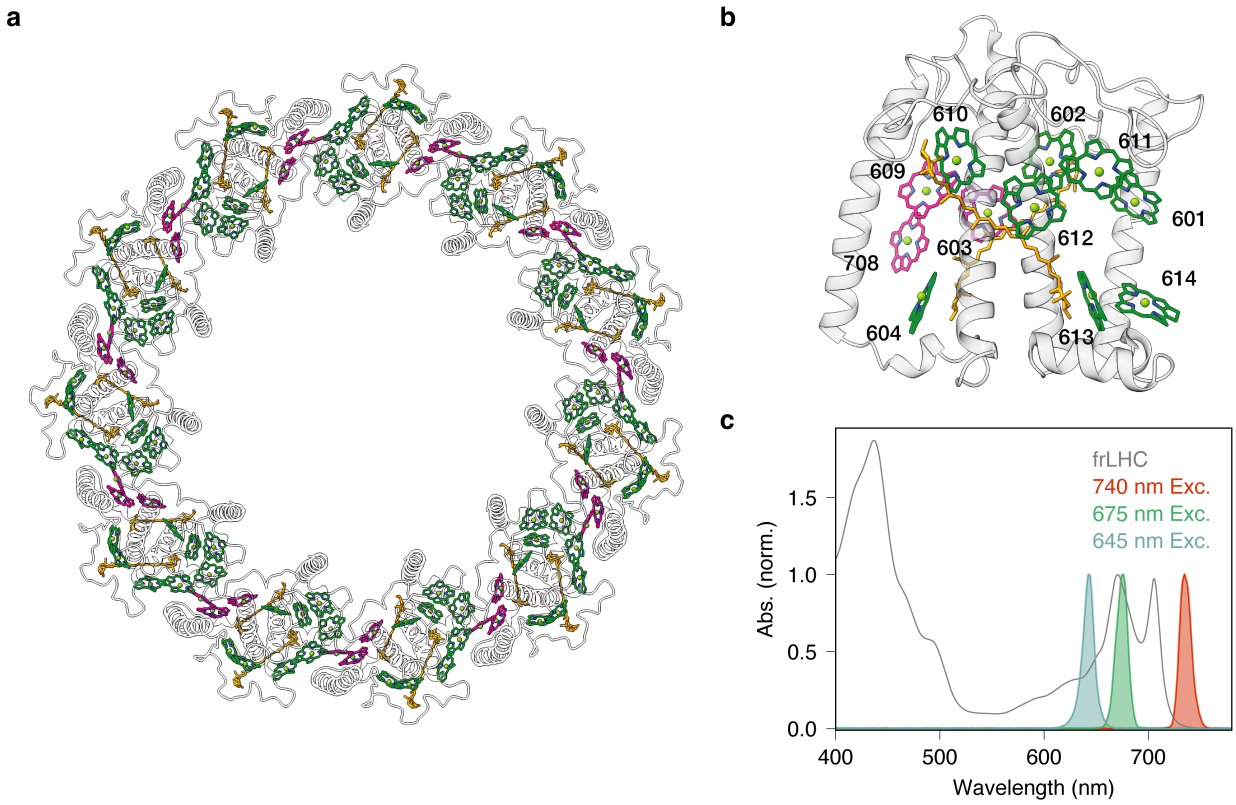

FIG. 1. (a) Undecameric structure of Pc-frLHC (PDB code 8HW1).[12] (b) Monomeric structure of Pc-frLHC. The monomer contains eleven Chls (green and magenta), two carotenoids (loroxanthin and violaxanthin; orange). The trimeric far-red Chls (603, 609 and 708) are shown in magenta. (c) Absorption spectra of Pc-frLHC in a buffer solution at room-temperature. The excitation laser spectra of transient absorption experiment are also shown.

II. EXPERIMENTAL

A. Ultrafast transient absorption spectroscopy.

The details of our transient absorption spectroscopy setup are reported elsewhere.[16] Briefly, the setup is based on a Yb:KGW regenerative amplifier (PHAROS-SP, Light Conversion, 1028 nm, 170 fs, 1 mJ, 6 kHz). The output of the amplifier is split into two parts. One part is used to generate the pump pulse, which is tunable over a broad wavelength range via home-built noncollinear optical parametric amplifiers (NOPAs).[17] In the present study, the seed pulse is passed through a 30 mm glass block to introduce chirp, resulting in spectral narrowing of the output. The pulse durations of the pump pulses, measured by SHG-FROG, were found to be shorter than 100 fs. The other part of the output of the amplifier is focused onto a 3 mm-thick sapphire plate using a lens to generate white-light continuum. This continuum is split into two beams, which serve as the probe and reference pulses. The polarization of the pump beam was set to the magic angle (54.7°) with respect to the probe pulse unless otherwise noted. Both the pump and probe beams were focused into a 500 μm-thick flow cell, in which the sample solution was continuously circulated. The transmitted probe pulse and reference pulse were analyzed using a pair of spectrometers, each composed of a prism, an achromatic lens, and a CMOS line camera (S12198-1024Q-01, Hamamatsu). The pump-induced absorbance change (ΔA) was measured on a shot-to-shot basis by mechanically chopping every other pump pulse. The typical beam diameter of the pump pulse at the sample position is ~170 μm ($1/e^2$ value), yielding an excitation fluence of ~1.5×10^{13} photons/pulse•cm^2 at 675 nm for a pulse energy of ~1.0 nJ. Chirp correction was performed based on the coherent artifact measurements using solvent only. Global analysis was performed using pyglotaran.[18]

B. Sample preparation.

Prasiola crispa culture strain 4113_Pc2 was used for the analysis.[19] The cells were cultivated onto 1.5% agar plate containing BG11 culture medium with HEPES adjusted to pH 7.5 with NaOH under 50 μmol photons m^{-2} s^{-1} fluorescence light at 15 °C for one month. To induce Pc-frLHC accumulation, cultivated cells were incubated in BG11 liquid medium (pH7.5) under 10 μmol photons m^{-2} s^{-1} far-red LED light with an emission peak at 730 nm at 15 °C for 1~2 weeks.

Cell disruption was performed with a ceramic ball mill (φ105 × 140 mm) and a beat bearer. Harvested cells were put into the ceramic pot with ceramic balls (φ10 ~ 15 mm) and the thylakoid buffer containing 25 mM MES-NaOH (pH 6.5), 12.5 % Glycerol, 1M betaine, 10 mM $MgCl_2$ and 5 mM EDTA. The pot was rolled by hand on ice for 15 min. Non-broken cells were separated as precipitation after a centrifugation at 700 ×g at 4ºC for 5 min. The supernatant was collected as thylakoid fraction. The precipitation was disrupted by bead beating with 0.5 mm zirconia/silica beads by using a bead beater (Bio Spec Products, Oklahoma, USA) with an attachments of plycarbonate Chamber Assemblies for 350 mL and an Ice Water Jacket. The bead beating condition was repeated 5 s beating and 2 min rest at 4ºC for 10 times. The suspension after the bead beating was centrifuged at 700 ×g at 4ºC for 5 min and the supernatant was collected as thylakoid fraction. All thylakoid fractions were put together and centrifuged with 20,000 ×g at 4ºC for 12 min and collected thylakoid membranes as the precipitation. The thylakoid membranes were solubilized with 1% (w/v) n-Dodecyl-β-D-maltoside (β-DDM) at a Chl concentration of 0.5 mg Chl/mL on ice for 20 min and centrifuged at 20,000 × g at 4ºC for 12 min. The supernatant was put on the sucrose density gradient (SDG) centrifugation with sucrose step gradient of 1, 0.8, 0.7, 0.6, 0.4, and 0.1 M with Buffer-B (25 mM MES, pH 6.5, 1 M betaine, 0.02% β-DDM) and fractionated by centrifugation with a swing rotor at 61,000 × g, at 4 °C for 24 h. The middle green band containing PSI-LHCI and Pc-frLHC was collected. The fraction was adsorbed on a diethylaminoethyl cellulose column (DE52; Whatman, Maidstone, UK), and PSI-LHCI was washed out with 150 mM NaCl containing Buffer-B. The

Pc-frLHC fraction was eluted with 250 mM NaCl containing Buffer-B, and concentrated by centrifugation with an angle rotor at 100,000 × g at 4 °C. The concentrated fraction was fractionated again by SDG centrifugation, and the lowest dark-green band was collected. The harvested fraction was diluted with Buffer B and concentrated by centrifugation at 100,000 × g at 4 °C.

III. RESULTS AND DISCUSSION

A. Transient absorption dynamics under three selective excitations reveals the excitonic level ordering.

We first investigated the excited-state dynamics of Pc-frLHC using a 740 nm pump pulse at low fluence, selectively exciting far-red Chls (FIG. 2a). Immediately after photoexcitation, a negative band centered at 710 nm was observed, corresponding to ground-state bleach (GSB) and stimulated emission (SE) of the far-red Chls. The GSB features from Chl *a* (680 nm) and Chl *b* (650 nm) were hardly observed, confirming that the excitation was specific to the far-red Chls. However, no significant spectral changes were observed on the picosecond timescale, suggesting that the uphill energy transfer processes may be too weak to be detected under these conditions.

To extract kinetic information, time traces of transient absorption at various probe wavelengths were globally analyzed based on a sequential model (FIG. 3a). We note that lifetime density analysis can be a powerful approach for heterogeneous systems;[20,21] however, our time resolution (~100 fs) is close to the fastest dynamics (~300 fs), and coherent artifacts hamper stable lifetime-density retrieval. We therefore base our kinetic discussion on the global analysis. Four components were required to fit the data, and the resulting evolution-associated difference spectra (EADS) are shown in FIG. 3b. The first two components, characterized by GSB and SE at 710 nm, evolve with time constants of 0.31 ps and 7.8 ps. These dynamics are accompanied by a slight blue shift in the SE region, which may reflect excitonic

relaxation or structural reorganization. The third-to-fourth transition, with a time constant of 140 ps, is characterized by a significant decrease in signal amplitude. A similar time constant was found in the previous time-resolved fluorescence study[12] and is tentatively assigned here to an increase in charge-transfer character, whereby an excitonic state with partial charge-transfer character ($Chl^{\delta+}$–$Chl^{\delta-}$) evolves into a state with stronger charge separation ($Chl^{\delta'+}$–$Chl^{\delta'-}$, where $\delta' > \delta$). A similar transition has also been reported in studies of molecular dyads and PSII reaction center.[22–24] The longest excited-state lifetime exceeds the detection limit of our setup (>1 ns).

Next, we examined the energy transfer dynamics upon excitation at 675 nm (FIG. 2b), which primarily excites Chl *a*. Following excitation, a negative band at 680 nm, corresponding to the GSB and SE of Chl *a*, emerged. It decayed within a few picoseconds, while a negative band at 708 nm emerged concomitantly, indicating the energy transfer from Chl *a* to far-red Chls. Global analysis yielded time constants of 0.31 ps, 2.3 ps, and 17 ps (FIG. 3d). The slowest component (17 ps) is similar to that observed in LHCII and is often attributed to energy transfer from a "bottleneck" site.[25,26] The intermediate component (2.3 ps) is assigned to the Chl *a*-to-far-red Chls energy transfer, as evidenced by the decrease of the Chl *a* GSB and the concomitant rise of the far-red Chl GSB in the EADS. The fastest component (0.31 ps) may also contribute to this transfer for the same reason, but is more likely to reflect excitonic relaxation within the far-red Chls, as will be discussed in detail later, supported by the delayed appearance of SE and the anisotropy dynamics. We note, however, that both the 0.31 ps and 2.3 ps components additionally include contributions from excitonic relaxation within the Chl *a* manifold and from energy transfer between blue- and red-absorbing Chl *a* sites, as the spectral shape of the GSB band at ~680 nm and its shoulder at ~670 nm evolves on this time scale.

Upon excitation at 645 nm, predominantly exciting Chl *b*, a pronounced negative band at 650 nm (GSB of Chl *b*) was observed (FIG. 2c and 3e, f). As this signal decayed, the Chl *a* signal remained

relatively unchanged, while the far-red Chls signal increased. Given the fast Chl *a*-to-far-red Chls transfer observed above, this suggests that energy from Chl *b* is relayed to far-red Chls via Chl *a*. In contrast to LHCII, no long-lived Chl *b* GSB component was detected on the picosecond timescale. In Pc-frLHC, most Chls are moderately coupled, except for Chl 604. This likely explains the absence of a "bottleneck" site for Chl *b*, in contrast to the presence of one for Chl *a*.

At early time delays (<500 fs), subtle spectral shifts were observed at the 710 nm band. A slight blue shift was detected upon 740 nm excitation (FIG. 2d), whereas a red shift with a time constant of ~310 fs occurred upon 675 nm excitation (FIG. 2e). This red shift reflects excitonic relaxation from a higher-lying excitonic state of the far-red Chls near ~670 nm to their lower-lying state at 710 nm, which produces the delayed appearance of SE around 710 nm. The nature and functional role of this higher-lying state will be addressed in detail later.

In addition, the residuals of the global fit exhibit clear oscillatory features at early delay times upon 740-nm excitation (FIG. 4a). Fourier transformation of the residuals yields a vibrational spectral map (FIG. 4b), which reveals a pronounced nodal pattern at ~710 nm corresponding to the GSB region of the far-red Chls. The dominant vibrational frequency is 78 cm^{-1} (FIG. 4c), in good agreement with a previous report on the bacterial reaction center that assigned a similar low-frequency mode to a protein vibrational wavepacket.[27] Because the energy of this mode is significantly smaller than the energy gaps involved in the Chl *a* manifold and in the excitonic manifold of the far-red Chls discussed below, we do not explore potential functional implications of this mode further in the present work.

Overall, the uphill energy transfer was not clearly resolved in the transient absorption measurement. This is likely due to the low thermal population of higher-energy Chl *a* states relative to far-red Chls. Considering the energy gap between Chl *a* (680 nm) and the far-red Chls (708 nm), which corresponds to

~580 cm^{-1}, the Boltzmann distribution predicts that the excited-state population of Chl *a* is only ~ 6% of that of the far-red Chls at room temperature, consistent with the experimental result.

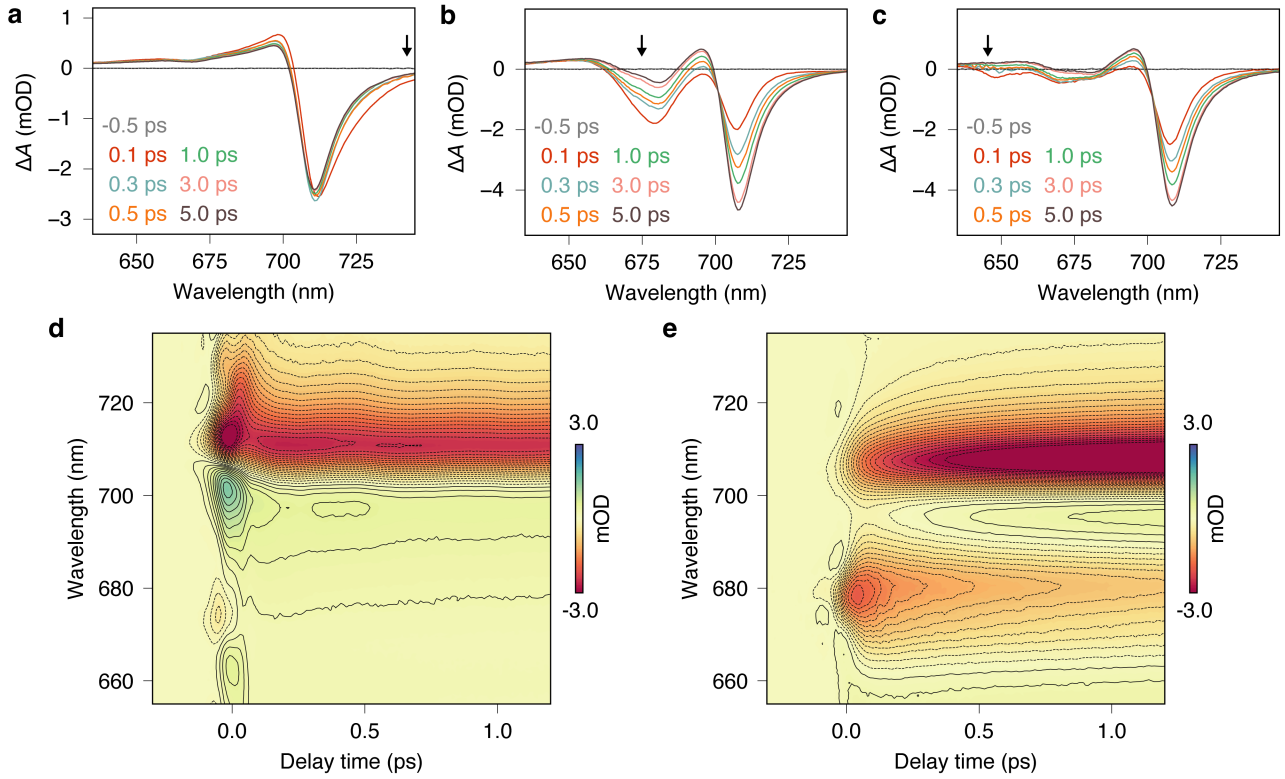

FIG. 2. Transient absorption spectra of Pc-frLHC upon the excitation at (a) 740 nm, (b) 675 nm, and (c) 645 nm. The excitation fluence was 10 nJ/pulse for 740 nm and 1 nJ/pulse for 675 nm and 645 nm. Black arrows indicate the center wavelength of the pump pulse. Contour plots of transient absorption spectra of Pc-frLHC excited at (d) 740 nm and (e) 675 nm.

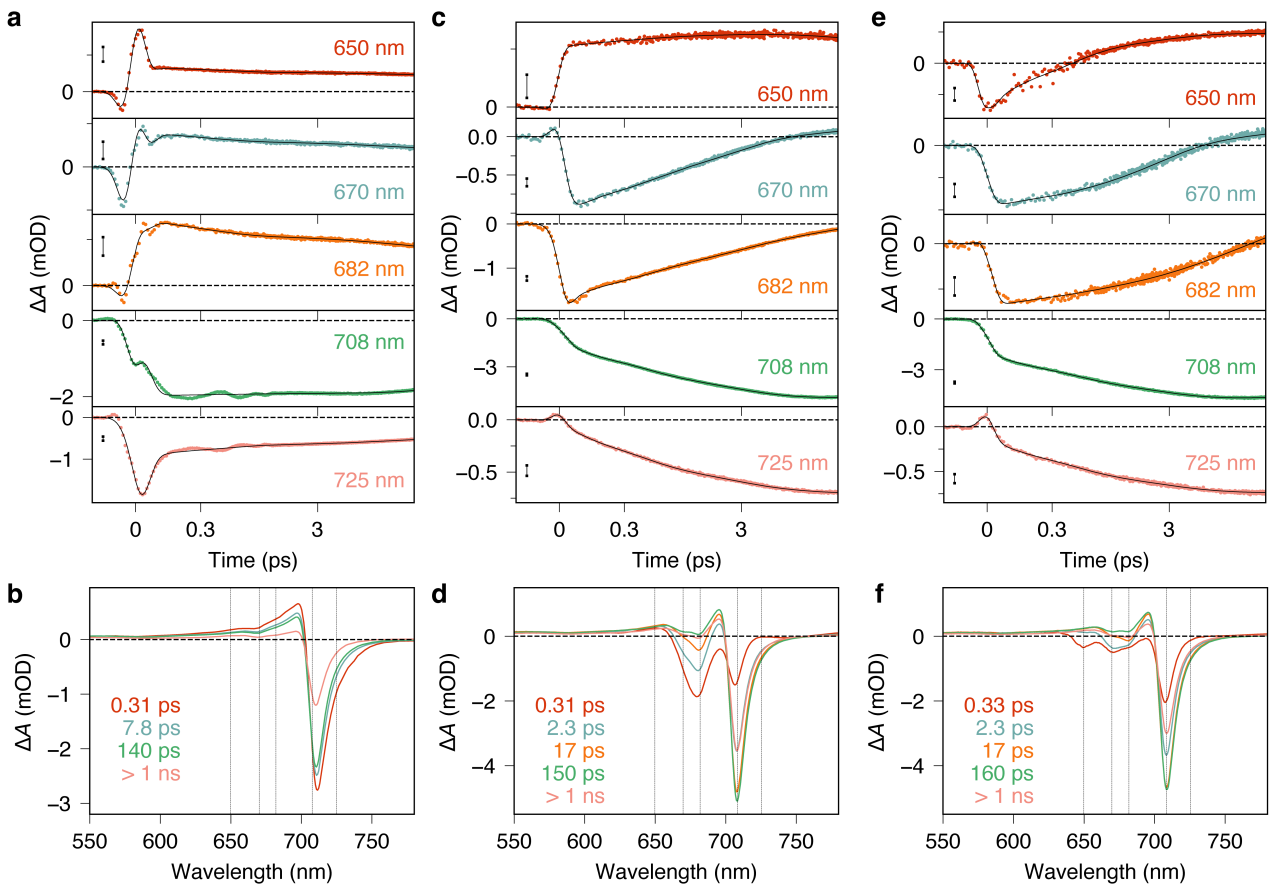

FIG. 3. Time-traces of transient absorbance of Pc-frLHC upon the excitation at (a) 740 nm, (c) 675 nm, and (e) 645 nm. The horizontal axis is linear until 0.3 ps and logarithmic at later delays. The scale bar indicates a range of 0.1 mOD. Black curve shows fitting result of global analysis. Evolution associated difference spectra of Pc-frLHC upon the excitation at (b) 740 nm, (d) 675 nm, and (f) 645 nm. Vertical black dotted line indicates the selected wavelength for time traces.

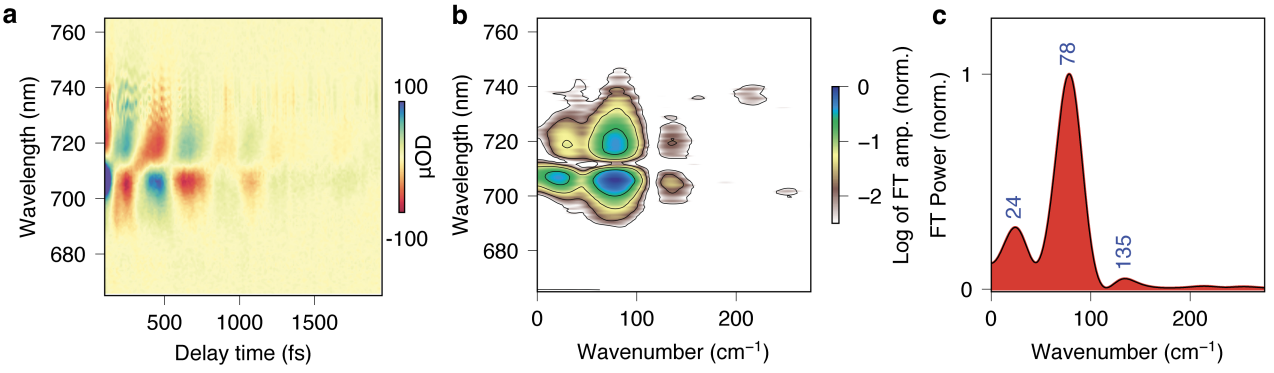

FIG. 4. (a) Residuals of the global analysis upon 740-nm excitation. (b) Vibrational spectral map obtained by Fourier transformation of the residuals, exhibiting a clear nodal pattern at ~710 nm corresponding to the GSB region of the far-red Chls. (c) Fourier-transform power spectrum integrated over the probe-wavelength window indicated in (b).

B. Uphill energy transfer corroborated by exciton–exciton annihilation dynamics.

To confirm the presence of uphill energy transfer, we examined the excitation fluence dependence of transient absorption dynamics in Pc-frLHC, focusing on far-red Chls. At high excitation densities, exciton–exciton annihilation, commonly observed in multichromophoric systems such as photosynthetic proteins, can occur.[28–31] In hopping-type energy transfer systems, annihilation occurs when two excitons encounter each other: one exciton transfers its energy to the other, promoting the acceptor to a higher excited state (S_n), which rapidly returns to the S_1 state, while the donor relaxes to the ground state. This process leads to a net depletion of the excited-state population and requires exciton diffusion. Therefore, observation of exciton–exciton annihilation serves as an indirect probe of exciton mobility around the undecameric Pc-frLHC ring, as well as of potential uphill energy-transfer pathways under conditions where only far-red-Chl excitons are created.

We investigated this phenomenon by exciting the sample at 740 nm with fluences ranging from 10 to 500 nJ/pulse (FIG. 5a). Transient absorption dynamics were monitored at 707 nm, which exhibits a quasi-isosbestic point in the picosecond regime (FIG 2a). At low excitation fluence, the signal exhibited a decay with a long lifetime (>100 ps). As the fluence increased, a rapid decay of the GSB was observed, indicative of exciton–exciton annihilation, facilitated by the uphill energy transfer and subsequent exciton diffusion around the undecameric ring. Notably, a fluence-dependent spectral change was also observed at an early delay time of 0.26 ps (FIG. 5b). At higher fluences (>100 nJ), a pronounced GSB signal

emerged at 670 nm, attributable to higher-energy Chl *a* or to a higher excitonic state of far-red Chls, indicating unintended multi-photon absorption that populates excitations other than the lowest excitonic state of the far-red Chls. Because this feature appears only at high fluence, it is more reasonably assigned to the population of higher-energy states rather than to a vibronic shoulder of the 708 nm band, which should be present even at low excitation levels. This interpretation is further supported by the 675-nm–excitation anisotropy data discussed below, which show distinct initial anisotropy values at 670 and 710 nm, behavior inconsistent with both signals originating from a vibronic progression. Consequently, the annihilation kinetics are influenced not only by uphill energy transfer but also by intra-monomer processes arising from multiple encounter channels at higher fluences; Chl *a*–Chl *a*, Chl *a*–far-red Chls, and multi-exciton interactions within the far-red Chl trimer.

Time traces were analyzed using multi-exponential fitting. Long-lived components (>100 ps) were fixed, and additional exponential terms were introduced when their relative amplitudes exceeded 0.1. Only the time constants related to annihilation are reported in Table 1. For fluences up to 30 nJ/pulse, the dynamics were adequately described by the long-lived components alone. Between 50 and 150 nJ, one additional short-lived component was required, with a time constant that decreased with increasing fluence. At fluences above 200 nJ, two short-lived components were necessary, with time constants ranging from 9.9 to 76 ps. To obtain a quantitative insight into the intrinsic annihilation dynamics, we analyzed the dependence of the annihilation rate on the excitation fluence (FIG. 5c). The apparent annihilation times exhibit a monotonic shortening with increasing excitation fluence within the weak-excitation regime (up to ~150 nJ in our case), as typically observed in exciton–exciton annihilation measurements. We therefore determined the intrinsic annihilation rate by linearly extrapolating the fluence-dependent rates to this regime, yielding $\tau_a^{-1} = 14.5\ ns^{-1}$ ($\tau_a = 69$ ps). Ideally, in an *N*-membered ring structure, the hopping time (τ_h) is related to the annihilation time as follows:[30]

$$\tau_a = \frac{\tau_h}{8\sin^2(\pi/2N)}. \quad (1)$$

Based on this relationship, the hopping time is estimated to be τ_h = 11.2 ps. In summary, these results suggest that the uphill energy transfer can be inferred from exciton–exciton annihilation dynamics. We note that the recently developed intensity-cycling approach provides a powerful framework for separating higher-order contributions by measuring transient absorption dynamics at multiple fluences.[32,33] In the present system, however, the spectral shape exhibits a clear dependence on excitation fluence (FIG. 5b), likely due to the limited spectral overlap between the pump spectrum and the absorption band of far-red Chls. This behavior complicates an unambiguous separation of different fifth-order pathways, including exciton–exciton annihilation and two-photon absorption, under our experimental conditions. Although ideal resonance conditions in which the annihilation-derived contribution dominates would enable a more definitive decomposition, this is not addressed in the present study. In the following section, we therefore employ transient absorption anisotropy measurements to further probe the timescale of the uphill energy transfer.

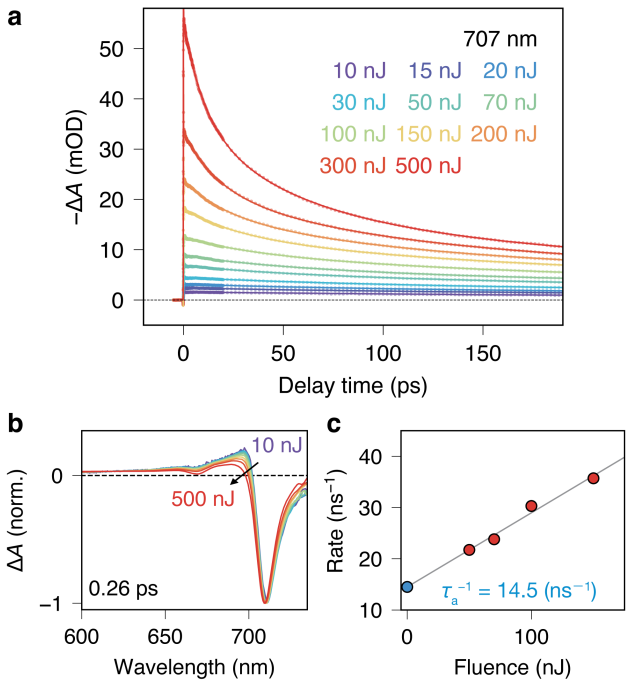

FIG. 5. (a) Time traces of transient absorbance of Pc-frLHC at 707 nm upon excitation at 740 nm with various fluences. The dots represent the experimental data, and the solid curves are multi-exponential fits. (b) Normalized transient absorption spectra at 0.26 ps. (c) Fluence dependence of the annihilation rate. The annihilation rate ($1/\tau_a$) extracted from multi-exponential fitting (TABLE 1) is plotted as a function of excitation fluence. A linear fit to the data provides an extrapolated low-fluence limit (blue dot), corresponding to the intrinsic annihilation rate, $\tau_a^{-1} = 14.5\ ns^{-1}$.

TABLE 1. Fitting results of transient absorption time traces at various excitation fluences. Only components with relative amplitude >0.1 are listed.

Fluence (nJ)	10~30	50	70	100	150	200	300	500
A_1	-	0.11	0.15	0.2	0.27	0.12	0.14	0.22
τ_1 (ps)	-	46	42	33	28	76	54	39
A_2	-	-	-	-	-	0.2	0.22	0.24
τ_2 (ps)	-	-	-	-	-	24	16	9.9

C. Transient anisotropy directly resolves the hopping time around the ring.

To further investigate the uphill energy transfer in Pc-frLHC, we performed transient absorption anisotropy measurements, which directly provide τ_h between the far-red Chls independent of nonlinear effects. Anisotropy measurements are a powerful means of probing energy transfer or electron/hole exchange between spectrally similar chromophores,[34,35] as commonly encountered in photosynthetic systems.[30,36–40] In this method, the anisotropy value is defined as

$$r(t) = \frac{\Delta A_{||}(t) - \Delta A_{\perp}(t)}{\Delta A_{||}(t) + 2\Delta A_{\perp}(t)}, \quad (2)$$

where $\Delta A_{\parallel}(t)$ and $\Delta A_{\perp}(t)$ are the transient absorption signals with probe polarization parallel and perpendicular to the pump, respectively. An initial anisotropy of 0.4 is expected when the transition dipole moments of excitation and probe transitions are perfectly aligned. Generally, the anisotropy value ranges between –0.2 and 0.4, depending on the relative angle θ between the dipole moments of the initially excited and probed transitions:

$$r(\theta) = \frac{3\cos^2\theta - 1}{5}. \quad (3)$$

Anisotropy decays over time due to depolarization processes, including rotational diffusion and energy transfer.

Upon one-photon excitation at 740 nm, the initial anisotropy at the GSB/SE region of the far-red Chls (710 nm) is approximately 0.4 (FIG. 6a). The ESA region (550–650 nm) shows anisotropy values ranging from 0.2 to 0.4. In particular, values lower than 0.4 indicate that the corresponding transition dipole moments are oriented differently. Remarkably, a value exceeding 0.4 was observed at 670 nm. Such an anomalously large anisotropy can occur in systems with degenerate electronic states or spectral overlap between positive and negative components (such as ESA and GSB),[39,41,42] as will be discussed in more detail below.

The anisotropy data were analyzed by performing global analysis simultaneously on the parallel and perpendicular signals ($\Delta A_{\parallel}(t)$ and $\Delta A_{\perp}(t)$) using shared time constants (FIG. 7). The resulting EADS were used to derive the evolution-associated anisotropy spectra (FIG. 7b). The time constants obtained were almost identical to those derived from the isotropic response (FIG. 3). Except at 670 nm, the anisotropy in most region decays to a residual value of ~0.1 with a dominant time constant of 9.8 ps. This residual anisotropy is consistent with in-plane dipolar relaxation[43] and has been reported in other ring-shaped systems, such as LH1 and LH2 complexes from purple bacteria,[37,38] as well as toroidal molecular aggregates.[35] Given that Pc-frLHC adopts a ring-shaped structure with symmetrically arranged far-red

Chls, the observed decay is attributed to depolarization due to energy migration within the ring, indicative of the uphill energy transfer. This depolarization can be modeled as exciton hopping around a circular array. For an undecameric ring ($N = 11$), the hopping time τ_h is related to the observed depolarization time τ_d as:[30,37]

$$\tau_d = \frac{\tau_h}{4\sin^2(2\pi/N)}. \quad (4)$$

This gives a hopping time between far-red Chls of $\tau_h \sim 11.5$ ps, in good agreement with the value estimated from the annihilation dynamics (~11.2 ps). The consistency between these independent approaches identifies 11.5 ps as the characteristic hopping time in Pc-frLHC. By contrast, in LH2, the hopping time is on the order of a few hundred femtoseconds,[30,37,38] which is consistent with the short B850 center-to-center spacing (~9 Å). In Pc-frLHC, the far-red Chls are separated by ~40 Å, suggesting that direct inter-trimer energy transfer is unlikely; instead, depolarization is plausibly mediated via uphill energy transfer through higher-energy Chl *a* sites in Pc-frLHC.

It is noteworthy that the anisotropy at 670 nm exceeded 0.4. Because this window overlaps the Chl *a* band, the anisotropy analysis resolves the presence of an upper excitonic state within the far-red Chl trimer. Although anisotropy typically ranges from –0.2 to 0.4, the observed value can deviate significantly when the signal consists of overlapping contributions. If the isotropic pump–probe signal at a given wavelength can be decomposed into two contributions, $\Delta A = \Delta A_A + \Delta A_B$, the observed anisotropy is the weighted average of the individual anisotropies; $r_{obs} = (\Delta A_A/(\Delta A_A + \Delta A_B))r_A + (\Delta A_B/(\Delta A_A + \Delta A_B))r_B$. Thus, the overlap between positive and negative contributions allows the anisotropy to take any real value ($-\infty < r < \infty$). Therefore, the signal at 670 nm indicates the overlapped contributions from the ESA and GSB, with the latter originating from an upper excitonic state of the far-red Chls that emerges upon 740 nm excitation.

This hypothesis is supported by anisotropy measurements with 675 nm excitation (FIG. 6b, FIG. 7c,d). Here, the anisotropy at 670 and 682 nm, assigned to a mixture of the upper excitonic state of the far-red Chls and Chl *a*, shows an initial value of approximately 0.4. In contrast, the anisotropy at 710 nm starts at ~0.2, suggesting that excitation at 675 nm generates a GSB that is distributed over the lower-energy far-red Chls excitonic state. This strongly supports the existence of an upper excitonic level of the far-red Chls near 670 nm. The anisotropy displays a biphasic decay with time constants of 290 fs and 2.3 ps. The slower component corresponds to energy transfer from Chl *a* to far-red Chls, which randomizes the excitation polarization and leads to near-zero anisotropy across most of the spectrum, except for the GSB region at 670–680 nm. The faster decay component likely reflects excitonic relaxation within the far-red Chls, as anisotropy decays from the first to the second spectral component across most wavelengths, again with the exception of the 670–680 nm GSB region. In the 670–680 nm GSB region, no significant change is observed within the first 290 fs. However, the anisotropy subsequently increases toward very large values (effectively diverging) as time progresses, then drops to –0.2 within ~15 ps, and continues to evolve over a timescale of ~150 ps. This behavior is attributed to the increasing signal intensity of the ESA that spectrally overlaps with the GSB. A similar persistence of non-zero anisotropy at long times has also been reported in LHCII.[36]

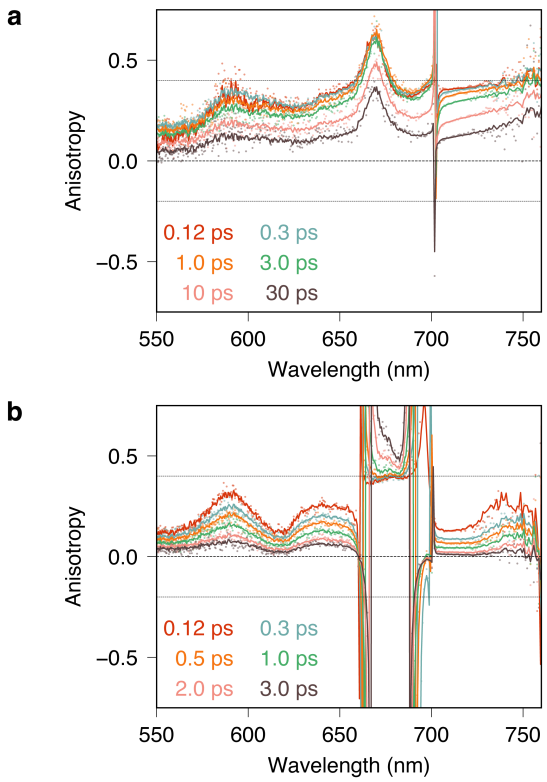

FIG. 6. (a) Anisotropy spectra of Pc-frLHC upon excitation at 740 nm. (b) Anisotropy spectra upon excitation at 675 nm. The dots show the raw data, and the solid lines represent global analysis fits. The black dotted lines indicate the 0.4 and –0.2 values.

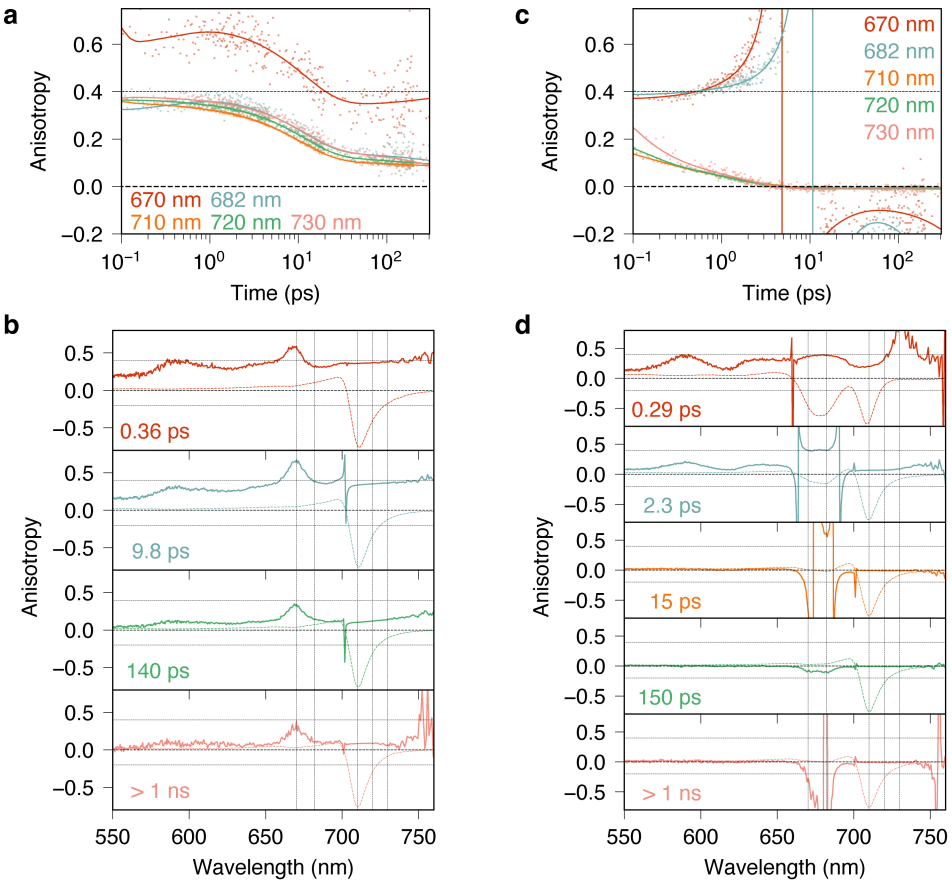

FIG. 7. (a) Time traces of anisotropy upon excitation at 740 nm. The dots show the experimental data, and the lines show global fits. (b) Evolution-associated anisotropy spectra. The dashed color curves represent the normalized isotropic response (ΔA). The vertical black dotted line indicates the selected wavelength for the time traces. The horizontal black dotted lines indicate the 0.4 and –0.2 values. (c–d) Corresponding results upon excitation at 675 nm.

D. Discussion on the functional role of the higher-lying excitonic state.

Multiple lines of evidence indicate the existence of a higher-lying excitonic state within the far-red Chls (FIG. 8a). Under 675 nm excitation, the ~710 nm SE grows with a delay, consistent with initial population of an upper state that rapidly (~0.3 ps) relaxes to the lowest level of far-red Chls (FIG. 2e). Transient absorption anisotropy measured under both 740 and 675 nm excitation further supports the

involvement of an upper state near ~670 nm; the unusually high anisotropy in this region (>0.4) under 740 nm excitation is explained by GSB–ESA spectral overlap associated with this state, while the modest anisotropy at ~710 nm (~0.2) under 675 nm excitation indicates GSB distribution across the lower-energy far-red excitonic level (FIG. 6 and 7). Taken together, these observations provide convergent evidence for a higher-lying far-red excitonic state that may contribute to energy redistribution within the complex. Such higher-lying excitonic states are known to play functional roles in multichromophoric systems like LH2, where they act as energy acceptors or mediators of energy equilibration.[44–48] In Pc-frLHC, we propose that the uphill transfer from the far-red Chls to Chl *a* (and onward to PSII) is facilitated by this upper state.

The ~800 cm^{-1} gap between the lower and upper levels of the far-red Chls corresponds to a small but finite thermal population (~2.1% at room temperature). Together with ultrafast relaxation and the uphill transfer time of ~11.5 ps, this enables repeated cycling during the ~2.2 ns excited-state lifetime,[12] i.e., providing many chances for the uphill transfer to Chl *a*. The 11.5 ps transfer time is reasonably close to the expectation from the Boltzmann distribution (~15 ps, inferred from the 0.31 ps) and aligns with the hopping times inferred from the exciton–exciton annihilation (~11.2 ps). Notably, if this higher-lying excitonic state were absent, direct uphill transfer from the far-red Chls to Chl *a* (across a smaller energy gap of ~580 cm^{-1}) would be slower (~38 ps, inferred from the 2.3 ps downhill transfer), despite a slightly higher thermal population (~6%). Such a rate is inconsistent with the experimentally constrained timescale of the exciton redistribution.

Importantly, the large energy separation (~800 cm^{-1}) between the far-red state (~710 nm) and the higher-energy state (~670 nm) does not reflect the excitonic coupling strength. Recent QM/MM calculations on the 603–609–708 trimer showed that these Chls possess substantial site-energy differences and exhibit pronounced charge-transfer character, which together strongly stabilize the lowest excitonic state.[15] As a consequence, a large energetic separation naturally arises between the lowest far-red state

(~710 nm) and the higher-energy excitonic states near 670 nm. In addition, previous work estimated that ~24% of the total Q_y intensity arises from the far-red Chls.[12] For a coupled system, excitonic mixing typically partitions the oscillator strength; when the lower and upper excitonic states share it in roughly a 2:1 ratio, the lower state would contribute ~18%, whereas a fully dark upper state would yield ~27%. The experimental value lies between these expectations. Because this estimate assumes equal oscillator strength for all eleven Chls, thereby underweighting Chl *a* relative to Chl *b* (whose extinction coefficient is lower), the oscillator strength of the far-red trimer, particularly its upper excitonic state(s), is likely underestimated. This indicates that the upper excitonic state(s) of the trimer cannot be spectroscopically dark and must retain appreciable oscillator strength.

In this work, we have operationally used the anisotropy-derived hopping time (τ_h ~ 11.5 ps) as a proxy for the uphill transfer time. This attribution is reasonable if uphill population exchange within the far-red Chls is the rate-limiting step that gates access to Chl *a*. In general, however, the hopping time emerges from an interplay of coupled processes: (i) intra-manifold equilibration among excitonic levels of the far-red Chls (including the upper ~670 nm state); (ii) inter-manifold transfer from far-red Chls to Chl *a*; (iii) intra-manifold migration within the Chl *a* manifold (Chl *a* ↔ Chl *a*); and (iv) inter-manifold transfer from Chl *a* to neighboring far-red Chls (e.g., in an adjacent subunit). Thus, τ_h primarily reflects depolarizing migration within the Pc-frLHC ring, not necessarily the donor→acceptor cross-manifold step. Accordingly, τ_h provides a characteristic upper bound (or at least a governing timescale) for the uphill transfer rather than a strict one-to-one measure.

Finally, the undecameric ring architecture (FIG. 8b) amplifies the above kinetic picture. Exciton hopping around the ring (τ_h ~ 11.5 ps) rapidly equilibrates the population of far-red Chls, so multiple subunits equivalently sample Chl *a*/PSII contact sites. This ring-wide equilibration, combined with upper-

state-assisted cycling, increases the overall probability that an excitation reaches Chl *a* before loss, providing a physical rationale for efficient PSII-directed energy flow under red-light conditions.

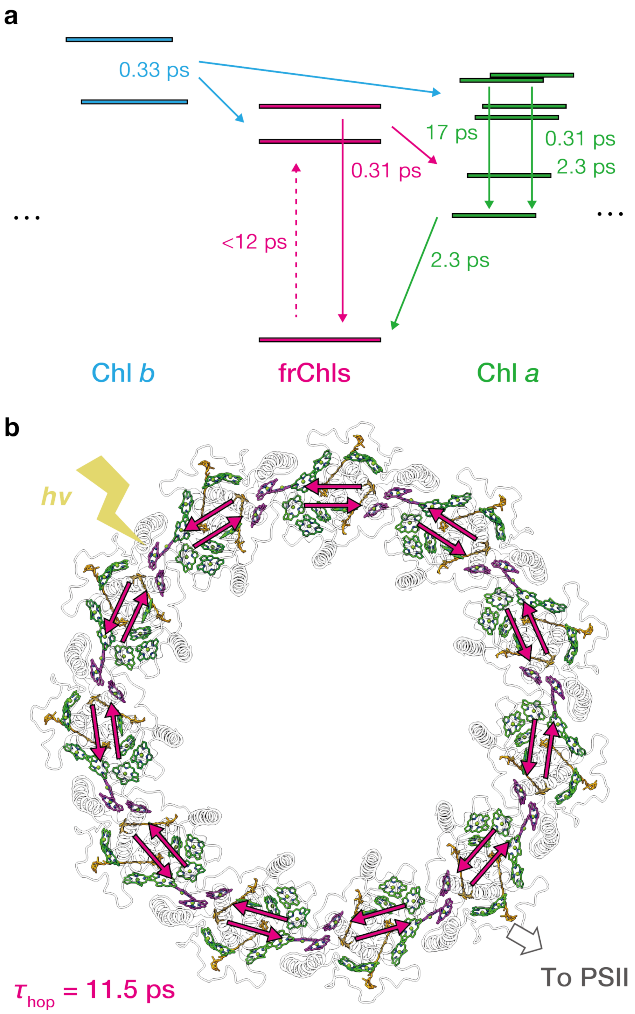

FIG. 8. (a) Schematic energy-level diagram summarizing the population flow among Chl *b* (blue), Chl *a* (green), and far-red Chls (frChls, magenta) in Pc-frLHC. (b) Structural cartoon of the undecameric, ring-shaped Pc-frLHC antenna. The magenta arrows indicate lateral exciton migration with a characteristic hopping time $\tau_h \sim 11.5$ ps.

IV. CONCLUSIONS

In this study, we elucidated the excitonic structure and energy transfer dynamics of the far-red light-harvesting complex from *P. crispa* (Pc-frLHC) using femtosecond transient absorption spectroscopy. Selective excitation of Chl *b*, Chl *a*, and far-red Chls revealed a rapid and directional cascade of energy transfer, culminating in population of the lowest excitonic state of the far-red Chl trimer. Exciton–exciton annihilation dynamics suggested a finite exciton mobility consistent with the uphill transfer, and transient absorption anisotropy measurements resolved a characteristic hopping time of ~11.5 ps, in good agreement with the annihilation-based estimate (~11.2 ps). Notably, a distinct excitonic state near 670 nm, supported by both anisotropy behavior and spectral dynamics, appears to facilitate repeated energy cycling and promote the thermally activated population transfer across the energy gap.

Despite the relatively large energy gap between the far-red Chls and Chl *a*, our data revealed clear signatures of the uphill energy transfer, likely mediated by a thermally populated higher-lying excitonic state within the far-red Chls. Together, these findings uncover a unique excitonic mechanism by which Pc-frLHC utilizes red-shifted photons to drive energy flow toward PSII. The presence of an upper excitonic level and the ring-shaped protein arrangement underpin an efficient energy transfer strategy, finely adapted to the light-limited interior of densely packed colonies, a characteristic niche of *P. crispa* in polar environments. These results provide broader insights into the design principles of photofunctional systems capable of exploiting low-energy light through excitonically mediated mechanisms.

ACKNOWLEDGMENTS

The culture strain of *Prasiola crispa* was a kind gift from Dr. Shuji Ohtani, Shimane University, Japan. We thank to Dr. Michael Hippler, University of Münster, Germany for his technical advice about the sample preparation. This work was partly supported by JSPS KAKENHI grant numbers JP21H05040, JP22K06380, JP23H04960, JP24H00452, JP24K01444, and 25K02338, JST FOREST Program grant

number JPMJFR201K, and the ExCELLS Special Collaboration Program of Exploratory Research Center on Life and Living Systems.

AUTHOR DECLARATIONS

Conflict of Interest

The authors have no conflicts to disclose.

Data Availability

The data that supports the findings of this study are available from the corresponding author upon reasonable request.

Author Contributions

Yusuke Yoneda: Conceptualization (equal); Formal analysis (lead); Funding acquisition (equal); Investigation (equal); Methodology (equal); Project administration (equal); Software (lead); Validation (equal); Visualization (lead); Writing – original draft (lead); Writing – review & editing (equal)

Makiko Kosugi: Conceptualization (equal); Funding acquisition (equal); Investigation (equal); Project administration (equal); Resources (equal); Validation (equal); Writing – original draft (supporting); Writing – review & editing (equal)

Jun Minagawa: Funding acquisition (equal); Resources (equal); Supervision (equal); Writing – review & editing (equal)

Hikaru Kuramochi: Funding acquisition (equal); Methodology (equal); Resources (equal); Supervision (equal); Writing – review & editing (equal)

REFERENCES

[1] R.E. Blankenship, *Molecular Mechanisms of Photosynthesis* (Blackwell Science Ltd, Oxford, UK, 2008).

[2] G.D. Scholes, G.R. Fleming, A. Olaya-Castro, and R. Van Grondelle, "Lessons from nature about solar light harvesting," Nat. Chem. **3**(10), 763–774 (2011).

[3] T. Mirkovic, E.E. Ostroumov, J.M. Anna, R. Van Grondelle, Govindjee, and G.D. Scholes, "Light absorption and energy transfer in the antenna complexes of photosynthetic organisms," Chem. Rev. **117**(2), 249–293 (2017).

[4] P. Joliot, A. Joliot, and B. Kok, "Analysis of the interactions between the two photosystems in isolated chloroplasts," Biochim. Biophys. Acta Bioenerg. **153**(3), 635–652 (1968).

[5] T. Morosinotto, M. Ballottari, F. Klimmek, S. Jansson, and R. Bassi, "The Association of the Antenna System to Photosystem I in Higher Plants," J. Biol. Chem. **280**(35), 31050–31058 (2005).

[6] M. Mozzo, M. Mantelli, F. Passarini, S. Caffarri, R. Croce, and R. Bassi, "Functional analysis of Photosystem I light-harvesting complexes (Lhca) gene products of Chlamydomonas reinhardtii," Biochim. Biophys. Acta Bioenerg. **1797**(2), 212–221 (2010).

[7] C. Wilhelm, and T. Jakob, "Uphill energy transfer from long-wavelength absorbing chlorophylls to PS II in Ostreobium sp. is functional in carbon assimilation," Photosynth. Res. **87**(3), 323 (2006).

[8] E. Kotabová, J. Jarešová, R. Kaňa, R. Sobotka, D. Bína, and O. Prášil, "Novel type of red-shifted chlorophyll a antenna complex from Chromera velia. I. Physiological relevance and functional connection to photosystems," Biochim. Biophys. Acta Bioenerg. **1837**(6), 734–743 (2014).

[9] B.M. Wolf, D.M. Niedzwiedzki, N.C.M. Magdaong, R. Roth, U. Goodenough, and R.E. Blankenship, "Characterization of a newly isolated freshwater Eustigmatophyte alga capable of utilizing far-red light as its sole light source," Photosynth. Res. **135**(1–3), 177–189 (2018).

[10] P.A. Broady, "Diversity, distribution and dispersal of Antarctic terrestrial algae," Biodivers. Conserv. **5**(11), 1307–1335 (1996).

[11] J. Seckbach, editor , *Algae and Cyanobacteria in Extreme Environments* (Springer Netherlands, Dordrecht, 2007).

[12] M. Kosugi, M. Kawasaki, Y. Shibata, K. Hara, S. Takaichi, T. Moriya, N. Adachi, Y. Kamei, Y. Kashino, S. Kudoh, H. Koike, and T. Senda, "Uphill energy transfer mechanism for photosynthesis in an Antarctic alga," Nat. Commun. **14**(1), 730 (2023).

[13] M. Kosugi, S.I. Ozawa, Y. Takahashi, Y. Kamei, S. Itoh, S. Kudoh, Y. Kashino, and H. Koike, "Red-shifted chlorophyll a bands allow uphill energy transfer to photosystem II reaction centers in an aerial green alga, Prasiola crispa, harvested in Antarctica," Biochim. Biophys. Acta Bioenerg. **1861**(2), 148139 (2020).

[14] M. Suga, S.-I. Ozawa, K. Yoshida-Motomura, F. Akita, N. Miyazaki, and Y. Takahashi, "Structure of the green algal photosystem I supercomplex with a decameric light-harvesting complex I," Nat. Plants **5**(6), 626–636 (2019).

[15] K. Saito, M. Kosugi, L. Qiu, J. Minagawa, and H. Ishikita, "Identification and design principles of far-red–absorbing chlorophyll in the light-harvesting complex," J. Biol. Chem. **301**(6), 108518 (2025).

[16] Y. Yoneda, T. Konishi, K. Suga, S. Saito, and H. Kuramochi, "Excited-State Aromatization Drives Nonequilibrium Planarization Dynamics," J. Am. Chem. Soc. **147**(14), 12051–12060 (2025).

[17] Y. Yoneda, and H. Kuramochi, "Rapid-Scan Resonant Two-Dimensional Impulsive Stimulated Raman Spectroscopy of Excited States," J. Phys. Chem. A **127**(24), 5276–5286 (2023).

[18] I.H.M. van Stokkum, J. Weißenborn, S. Weigand, and J.J. Snellenburg, "Pyglotaran: a lego-like Python framework for global and target analysis of time-resolved spectra," Photochem. Photobiol. Sci. **22**(10), 2413–2431 (2023).

[19] M. Kosugi, S. Ohtani, K. Hara, A. Toyoda, H. Nishide, S.-I. Ozawa, Y. Takahashi, Y. Kashino, S. Kudoh, H. Koike, and J. Minagawa, "Characterization of the far-red light absorbing light-harvesting

chlorophyll a/b binding complex, a derivative of the distinctive Lhca gene family in green algae," Front. Plant. Sci. **15**, 1409116 (2024).

[20] R. Croce, M.G. Müller, R. Bassi, and A.R. Holzwarth, "Carotenoid-to-Chlorophyll Energy Transfer in Recombinant Major Light-Harvesting Complex (LHCII) of Higher Plants. I. Femtosecond Transient Absorption Measurements," Biophys. J. **80**(2), 901–915 (2001).

[21] A.R. Holzwarth, M.G. Müller, M. Reus, M. Nowaczyk, J. Sander, and M. Rögner, "Kinetics and mechanism of electron transfer in intact photosystem II and in the isolated reaction center: Pheophytin is the primary electron acceptor," Proc. Natl. Acad. Sci. U.S.A. **103**(18), 6895–6900 (2006).

[22] E. Takeuchi, M. Muramatsu, T. Katayama, Y. Yoneda, S. Ito, Y. Nagasawa, and H. Miyasaka, "Sub-100 fs Charge Separation and Subsequent Diffusive Solvation Observed for Asymmetric Bianthryl Derivative in Ionic Liquid," J. Phys. Chem. C **120**(27), 14502–14512 (2016).

[23] Y. Yoneda, S.J. Mora, J. Shee, B.L. Wadsworth, E.A. Arsenault, D. Hait, G. Kodis, D. Gust, G.F. Moore, A.L. Moore, M. Head-Gordon, T.A. Moore, and G.R. Fleming, "Electron-Nuclear Dynamics Accompanying Proton-Coupled Electron Transfer," J. Am. Chem. Soc. **143**(8), 3104–3112 (2021).

[24] Y. Yoneda, E.A. Arsenault, S.-J. Yang, K. Orcutt, M. Iwai, and G.R. Fleming, "The initial charge separation step in oxygenic photosynthesis," Nat. Commun. **13**(1), 2275 (2022).

[25] R. van Grondelle, and V.I. Novoderezhkin, "Energy transfer in photosynthesis: experimental insights and quantitative models," Phys. Chem. Chem. Phys. **8**(7), 793–807 (2006).

[26] A.D. Stahl, M. Di Donato, I. Van Stokkum, R. Van Grondelle, and M.L. Groot, "A femtosecond visible/visible and visible/mid-infrared transient absorption study of the light harvesting complex II," Biophys. J. **97**(12), 3215–3223 (2009).

[27] M.H. Vos, F. Rappaport, J.-C. Lambry, J. Breton, and J.-L. Martin, "Visualization of coherent nuclear motion in a membrane protein by femtosecond spectroscopy," Nature **363**(6427), 320–325 (1993).

[28] T. Gillbro, Å. Sandström, M. Spangfort, V. Sundström, and R. van Grondelle, "Excitation energy annihilation in aggregates of chlorophyll ab complexes," Biochim. Biophys. Acta Bioenerg. **934**(3), 369–374 (1988).

[29] V. Barzda, V. Gulbinas, R. Kananavicius, V. Cervinskas, H. Van Amerongen, R. Van Grondelle, and L. Valkunas, "Singlet–Singlet Annihilation Kinetics in Aggregates and Trimers of LHCII," Biophys. J. **80**(5), 2409–2421 (2001).

[30] G. Trinkunas, J.L. Herek, T. Polívka, V. Sundström, and T. Pullerits, "Exciton Delocalization Probed by Excitation Annihilation in the Light-Harvesting Antenna LH2," Phys. Rev. Lett. **86**(18), 4167–4170 (2001).

[31] Y. Yoneda, T. Katayama, Y. Nagasawa, H. Miyasaka, and Y. Umena, "Dynamics of Excitation Energy Transfer Between the Subunits of Photosystem II Dimer," J. Am. Chem. Soc. **138**(36), 11599–11605 (2016).

[32] P. Malý, J. Lüttig, P.A. Rose, A. Turkin, C. Lambert, J.J. Krich, and T. Brixner, "Separating single- from multi-particle dynamics in nonlinear spectroscopy," Nature **616**(7956), 280–287 (2023).

[33] J.J. Krich, L. Brenneis, P.A. Rose, K. Mayershofer, S. Büttner, J. Lüttig, P. Malý, and T. Brixner, "Separating Orders of Response in Transient Absorption and Coherent Multidimensional Spectroscopy by Intensity Variation," J. Phys. Chem. Lett. **16**(24), 5897–5905 (2025).

[34] H. Miyasaka, T. Moriyama, and A. Itaya, "Direct Detection of Hole Migration along the Polymer Chain: Poly(N -vinylcarbazole) in 1,2-Dichloroethane Solution As Revealed by Picosecond Transient Absorption and Dichroism Measurements," J. Phys. Chem. **100**(30), 12609–12615 (1996).

[35] S. Takahashi, T. Matsumoto, M.J. Hollamby, H. Miyasaka, M. Vacha, H. Sotome, and S. Yagai, "Impact of Ring-Closing on the Photophysical Properties of One-Dimensional π-Conjugated Molecular Aggregate," J. Am. Chem. Soc. **146**(3), 2089–2101 (2024).

[36] S. Savikhin, H. van Amerongen, S.L. Kwa, R. van Grondelle, and W.S. Struve, "Low-temperature energy transfer in LHC-II trimers from the Chl a/b light-harvesting antenna of photosystem II," Biophys. J. **66**(5), 1597–1603 (1994).

[37] S.E. Bradforth, R. Jimenez, F. van Mourik, R. van Grondelle, and G.R. Fleming, "Excitation Transfer in the Core Light-Harvesting Complex (LH-1) of Rhodobacter sphaeroides: An Ultrafast Fluorescence Depolarization and Annihilation Study," J. Phys. Chem. **99**(43), 16179–16191 (1995).

[38] R. Jimenez, S.N. Dikshit, S.E. Bradforth, and G.R. Fleming, "Electronic Excitation Transfer in the LH2 Complex of Rhodobacter sphaeroides," J. Phys. Chem. **100**(16), 6825–6834 (1996).

[39] D.M. Jonas, M.J. Lang, Y. Nagasawa, T. Joo, and G.R. Fleming, "Pump−Probe Polarization Anisotropy Study of Femtosecond Energy Transfer within the Photosynthetic Reaction Center of Rhodobacter sphaeroides R26," J. Phys. Chem. **100**(30), 12660–12673 (1996).

[40] T. Pullerits, M. Chachisvilis, and V. Sundström, "Exciton Delocalization Length in the B850 Antenna of Rhodobacter sphaeroides," J. Phys. Chem. **100**(25), 10787–10792 (1996).

[41] K. Wynne, and R.M. Hochstrasser, "Coherence effects in the anisotropy of optical experiments," Chem. Phys. **171**(1–2), 179–188 (1993).

[42] C. Galli, K. Wynne, S.M. LeCours, M.J. Therien, and R.M. Hochstrasser, "Direct measurement of electronic dephasing using anisotropy," Chem. Phys. Lett. **206**(5–6), 493–499 (1993).

[43] D. Magde, "Photoselection with intense laser pulses," J. Chem. Phys. **68**(8), 3717–3733 (1978).

[44] V. Nagarajan, R.G. Alden, J.C. Williams, and W.W. Parson, "Ultrafast exciton relaxation in the B850 antenna complex of Rhodobacter sphaeroides," Proc. Natl. Acad. Sci. U.S.A. **93**(24), 13774–13779 (1996).

[45] X. Hu, T. Ritz, A. Damjanović, and K. Schulten, "Pigment Organization and Transfer of Electronic Excitation in the Photosynthetic Unit of Purple Bacteria," J. Phys. Chem. B **101**(19), 3854–3871 (1997).

[46] R.G. Alden, E. Johnson, V. Nagarajan, W.W. Parson, C.J. Law, and R.G. Cogdell, "Calculations of Spectroscopic Properties of the LH2 Bacteriochlorophyll−Protein Antenna Complex from Rhodopseudomonas acidophila," J. Phys. Chem. B **101**(23), 4667–4680 (1997).

[47] K. Mukai, S. Abe, and H. Sumi, "Theory of Rapid Excitation-Energy Transfer from B800 to Optically-Forbidden Exciton States of B850 in the Antenna System LH2 of Photosynthetic Purple Bacteria," J. Phys. Chem. B **103**(29), 6096–6102 (1999).

[48] Y. Yoneda, T. Noji, N. Mizutani, D. Kato, M. Kondo, H. Miyasaka, Y. Nagasawa, and T. Dewa, "Energy transfer dynamics and the mechanism of biohybrid photosynthetic antenna complexes chemically linked with artificial chromophores," Phys. Chem. Chem. Phys. **24**(40), 24714–24726 (2022).